

Trajectory Reconstruction of the ST-9 Sounding Rocket Experiment Using IMU and Landmark Data

Ryan S. Park*, Shyam Bhaskaran[†], John J. Bordi[‡], Yang Cheng[§], Andrew J. Johnson[¶],
Gerhard L. Kruijzinga^{||}, Michael E. Lisano^{**}, William M. Owen^{††} and Aron A. Wolf^{‡‡}
Jet Propulsion Laboratory, California Institute of Technology, Pasadena, California, 91109

This paper presents trajectory reconstruction of the ST-9 sounding rocket experiment using the onboard IMU data and descent imagery. The raw IMU accelerometer measurements are first converted into inertial acceleration and then used in trajectory integration. The descent images are pre-processed using a map-matching algorithm and unique landmarks for each image are created. Using the converted IMU data and descent images, the result from dead-reckoning and the kinematic-fix approaches are first compared with the GPS measurements. Then, both the IMU data and landmarks are processed together using a batch least-squares filter and the position, velocity, stochastic acceleration, and camera orientation of each image are estimated. The reconstructed trajectory is compared with the GPS data and the corresponding formal uncertainties are presented. The result shows that IMU data and descent images processed with a batch filter algorithm provide the trajectory accuracy required for pin-point landing.

I. Nomenclature

a	=	distance from a camera to landmark vector
$\hat{\mathbf{a}}^C$	=	unit-vector from a camera to the center of each pixel in camera frame
f	=	camera focal length
N	=	number of measurements
\mathbf{h}_k	=	measurement partial vector
p_k, l_k	=	pixel and line, respectively
p_0, l_0	=	center of the pixel/line space
p_r, l_r	=	camera pixel and line resolutions, respectively
p_f, l_f	=	pixel and line field-of-view sizes, respectively
\mathbf{r}^B	=	spacecraft position vector in Earth-fixed frame

*Member of Engineering Staff, Outer Planet Navigation Group, Jet Propulsion Laboratory, Pasadena, California, Member AAS, Senior Member AIAA, Ryan.S.Park@jpl.nasa.gov.

[†]Group Supervisor, Outer Planet Navigation Group, Jet Propulsion Laboratory, Pasadena, California, Shyam.Bhaskaran@jpl.nasa.gov.

[‡]Senior Member of Engineering Staff, Outer Planet Navigation Group, Jet Propulsion Laboratory, Pasadena, California, John.J.Bordi@jpl.nasa.gov.

[§]Senior Member of Engineering Staff, Computer Vision Group, Jet Propulsion Laboratory, Pasadena, California, Yang.Cheng@jpl.nasa.gov.

[¶]Senior Member of Engineering Staff, Optical Navigation Group, Jet Propulsion Laboratory, Pasadena, California, Andrew.E.Johnson@jpl.nasa.gov.

^{||}Senior Member of Engineering Staff, Inner Planet Navigation Group, Jet Propulsion Laboratory, Pasadena, California, Gerhard.L.Kruijzinga@jpl.nasa.gov.

^{**}Group Supervisor, Orbiter Missions System Engineering Group, Jet Propulsion Laboratory, Pasadena, California, Michael.E.Lisano@jpl.nasa.gov.

^{††}Group Supervisor, Optical Navigation Group, Jet Propulsion Laboratory, Pasadena, California, Member AAS, William.M.Owen@jpl.nasa.gov.

^{‡‡}Group Supervisor, EDL/Aero Applications Group, Jet Propulsion Laboratory, Pasadena, California, Aron.A.Wolf@jpl.nasa.gov.

©2009 California Institute of Technology. Government sponsorship acknowledged.

$\mathbf{r}_{\text{imk}}^{\text{B}}$	=	landmark vector in Earth-fixed frame
\mathbf{R}_{CB}	=	rotation matrix from Earth-fixed to camera frame
\mathbf{W}_k	=	measurement weight matrix
x, y	=	pixel/line location in mm space coordinates
\mathbf{z}_k	=	k^{th} landmark measurement
\mathbf{z}_k^*	=	k^{th} actual measurement
α, δ, ϕ	=	camera orientation angle (right ascension, declination, and twist)
Λ_0	=	epoch state information matrix

II. Introduction

The ST-9 sounding rocket experiment, also known as 41.068, was launched on April 5, 2006 from White Sands Missile Range, New Mexico. It was a part of NASA's space technology program which was intended to demonstrate pin-point landing capability, where the pin-point landing assumes landing uncertainties within 100 meters.¹ Such an experiment is crucial for future space missions, such as the proposed Mars Sample Return, which require high-precision landing and/or hazard avoidance.

The launch vehicle was a two-stage rocket system (Terrier-Orion) and the payload was equipped with an Inertial Measurement Unit (IMU), a Global Positioning System (GPS) receiver, and two digital cameras. The first camera was an analog video recorder which directly down-linked the telemetry to the ground receiver during the flight. The second camera was a digital video recorder which stored data onboard and transferred the data to a telemetry payload for downlink, which had higher risk of hardware failure. This paper uses the descent images from the analog camera. From launch to landing took little over 800 seconds in flight time and Figure 1 depicts a cartoon showing the mission scenario.

The ST-9 trajectory was first analyzed by Mourikis *et al.* where the IMU data and descent images were sequentially processed using the extended Kalman filter (EKF) algorithm.² Moreover, they provide a detailed experiment profile and thorough analysis on the expected estimation performance. The purpose of this paper is to demonstrate that both IMU data and images can be processed using a batch filter algorithm, which is fundamentally different from the sequential algorithm and has been used in trajectory navigation for many decades.³ In practice, navigators favor a batch filter over a sequential filter due to easier data editing, mapping, smoothing, etc. This paper shows that the 100-meter pin-point landing requirement can be achieved using IMU and landmark data with a batch filter algorithm, and that it can be implemented as an onboard navigation filter.

In this study, the raw IMU accelerometer data are first converted into inertial accelerations. The spacecraft trajectory is then integrated using the converted IMU data and the difference is compared with GPS measurements, which are assumed to be the truth. The descent images are pre-processed using a map-matching algorithm and unique landmarks for each image are created. Using the mapped landmarks, the position and attitude at the measurement times are computed using a kinematic-fix algorithm and are compared with the GPS position and the dead-reckoned spacecraft attitude. Finally, both IMU and landmark data are combined in a full least-squares batch filter, where the position, velocity, stochastic acceleration, and camera orientation angle are estimated. The estimated trajectory is compared with the GPS measurements, and the reconstruction error and corresponding formal uncertainties are presented.

III. Data Calibration

This section presents calibration of the ST-9 IMU data and descent imagery that are used in the trajectory reconstruction.

A. Inertial Measurement Unit

The raw IMU accelerometer data is given in the spacecraft frame. The accelerometer data is first rotated into the inertial EME2000 frame using the dead-reckoned IMU gyro data and a high-precision Earth orientation model. The non-gravitational acceleration profile is saved at 50 Hz. The onboard IMU outputs the data at a higher rate, but the 41.068 flight system implementation did not allow rates higher than 50 Hz. Figure 2(a) shows the converted IMU accelerometer data, which is used in trajectory integration.

The integration model is based on an 8×8 Earth gravity field and IMU acceleration data, and JPL's Orbit Determination Program (ODP) is used to integrate the trajectory. Figure 2(b) shows the position and velocity differences

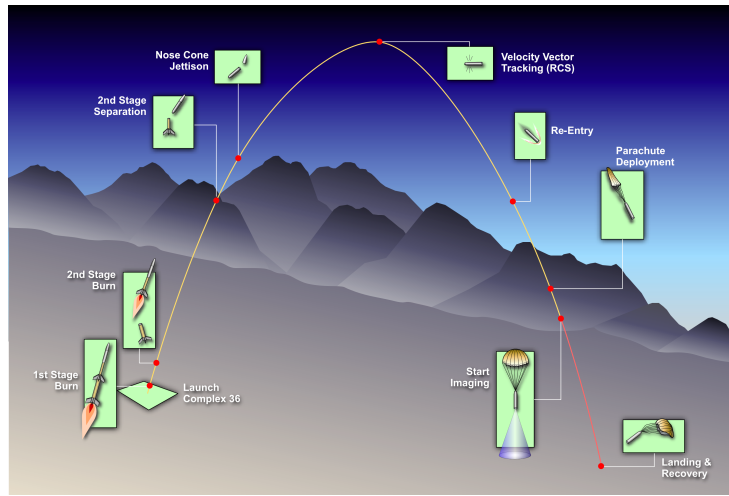
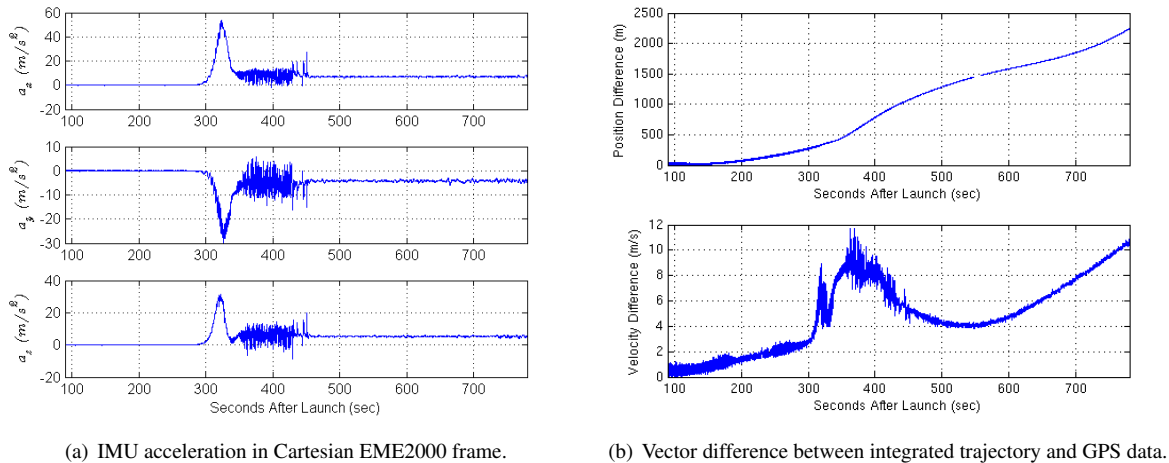


Figure 1. Mission scenario of the ST-9 sounding rocket experiment.

between the integrated and GPS trajectories. Note that the trajectory is integrated starting 90 seconds after launch, which is after the Terrier and Orion separations, and is initialized with the corresponding GPS state. The trajectory reached the maximum altitude of about 120 km and the maximum velocity of about 1.25 km/s. The result shows that the dead-reckoned trajectory using IMU data yields errors of ~ 2.3 km and ~ 11 m/s for position and velocity, respectively, which clearly does not satisfy the pin-point landing accuracy of 100 meters. When combined with optical data, however, this error will be significantly reduced, which will be discussed later in this paper. Note that this high error is mainly due to the noisy IMU data, and in actual flight missions, the noise level can be reduced and calibrated depending on the choice of an IMU payload.⁴



(a) IMU acceleration in Cartesian EME2000 frame.

(b) Vector difference between integrated trajectory and GPS data.

Figure 2. Dead-reckon result using IMU data only.

B. Map-Matching Algorithm

The ST-9 image data are processed using the Map And Image Alignment (MAIA) algorithm.² The MAIA algorithm aims to match landmarks (LM) between descent images and a base map, which is an ortho-rectified aerial, or orbital image. This consists of two steps: fast Fourier transform (FFT) map matching and mapped landmark matching. Figure 3 shows the base map used in this study. Because of very large uncertainty of initial horizontal position and the relatively small attitude and altitude error, a rough horizontal correction is needed in order to speed up the data process.

The FFT-base map matching is used to provide a rough horizontal position estimate. Then a descent image can be warped roughly to its corresponding location on the base map. Due to several factors, such as position or attitude error and terrain relief, the warped descent image does not always match perfectly with the base map. Therefore, map landmark matching is used to correct the small error. In this step, multiple templates (i.e., landmarks) are selected in the descent image and then they are warped to the base map. An image spatial correlation is used to determine their correspondents in the base map.²

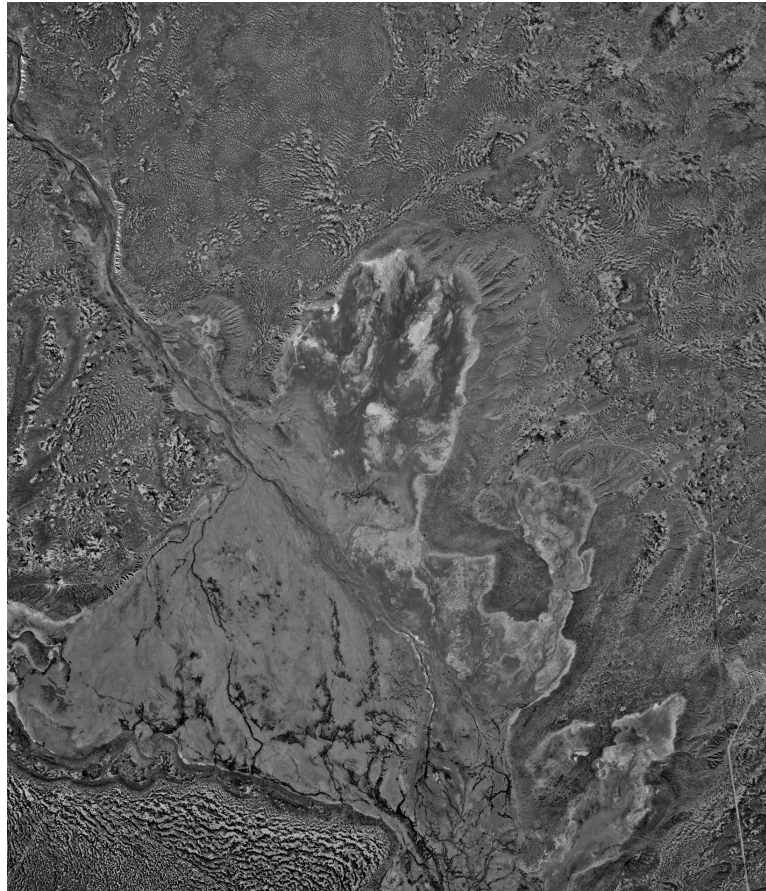


Figure 3. Base map figure.

The base map used here is a USGS Orthophoto Quadrangles (DOQs) map named Lumley Lake. It is a Universal Transverse Mercator (UTM) projected 1-meter aerial image in NAD83. The landmark elevation is obtained using Shuttle Radar Topography Mission (SRTM) elevation data of the same area. This Digital Elevation Map (DEM) is stored in simple latitude and longitude grids with a roughly 3-arc-second grid-size. In order to retrieve the elevation data, the landmark position in the base map is converted from UTM coordinates to geographic coordinates and its elevation is interpolated from the DEM data. A small elevation correction (-22.3 meters) is applied to each elevation due to the difference between NGA EGM96 and WGS 84.⁵ Finally, the landmarks are converted into Earth body-fixed 3D positions.

C. Kinematic-Fix of Landmark Data

Landmark tracking is a powerful data type which provides body-relative positional and angular information about the trajectory. Typically, tens of landmarks are provided per image, but in theory, only three landmarks are needed to determine the position and attitude at the time of measurement. More landmarks basically improve the measurement accuracy by $\mathcal{O}(\sqrt{N})$. The process of determining the position and attitude given landmarks is called the kinematic-fix technique. It is based on the least-squares principle, and depending on the accuracy of the landmarks, a high-precision body-relative estimate can be obtained.⁶

Given pixel/line data with corresponding landmarks, the goal of kinematic-fix is to compute the body-fixed (Earth-fixed in this study) position vector \mathbf{r}^B and camera orientation angles (α , δ , and ϕ) at the time the image is taken. The camera orientation angles define the spacecraft-to-camera frame rotation matrix, which can be stated as:

$$\mathbf{R}_{CB} = \begin{bmatrix} +\cos\alpha\sin\delta\cos\phi - \sin\alpha\sin\phi & +\sin\alpha\sin\delta\cos\phi + \cos\alpha\sin\phi & -\cos\delta\cos\phi \\ -\cos\alpha\sin\delta\sin\phi - \sin\alpha\cos\phi & -\sin\alpha\sin\delta\sin\phi + \cos\alpha\cos\phi & +\cos\delta\sin\phi \\ +\cos\alpha\cos\delta & +\sin\alpha\cos\delta & +\sin\delta \end{bmatrix}, \quad (1)$$

where α and δ denote camera bore-sight right ascension and declination, respectively, and ϕ denotes the camera twist angle. Note that \mathbf{R}_{CB} is simply a 3-2-3 sequence of direction cosine matrices, i.e., $\mathbf{R}_z(\phi)\mathbf{R}_y(90^\circ - \delta)\mathbf{R}_x(\alpha)$,^a and the camera orientation angles can be computed as:

$$\alpha = \tan^{-1}(\mathbf{R}_{CB}^{32}/\mathbf{R}_{CB}^{31}), \quad (2)$$

$$\delta = \sin^{-1}\mathbf{R}_{CB}^{33}, \quad (3)$$

$$\phi = \tan^{-1}(-\mathbf{R}_{CB}^{23}/\mathbf{R}_{CB}^{13}). \quad (4)$$

A landmark measurement (\mathbf{z}_k) of an image is simply the pixel/line combination, i.e.,

$$\mathbf{z}_k = \begin{bmatrix} p_k \\ l_k \end{bmatrix}, \quad (5)$$

where p_k and l_k represent pixel and line, respectively.^b Given landmark measurements, Earth-fixed position and camera orientation angles can be estimated iteratively by solving the following normal equation:^{7,8}

$$\tilde{\mathbf{z}} = \mathbf{\Lambda}_0 \cdot \delta\mathbf{x}_0, \quad (6)$$

where

$$\mathbf{\Lambda}_0 = \sum_{k=1}^N \mathbf{h}_k^T \mathbf{W}_k \mathbf{h}_k, \quad (7)$$

$$\tilde{\mathbf{z}} = \sum_{k=1}^N \mathbf{h}_k^T \mathbf{W}_k [\mathbf{z}_k^* - \mathbf{z}_k(\mathbf{r}^B, \alpha, \delta, \phi)]. \quad (8)$$

Note that the measurement partial vector is defined as $\mathbf{h}_k = \partial(p_k, l_k)/\partial(\mathbf{r}^B, \alpha, \delta, \phi)$.

In order to compute \mathbf{h}_k , first define the pixel/line location (x, y) in camera (mm) coordinates:

$$\begin{bmatrix} x \\ y \end{bmatrix} = \mathbf{K}^{-1} \begin{bmatrix} p - p_0 \\ l - l_0 \end{bmatrix}, \quad (9)$$

where p_0 and l_0 represent the origin of the pixel/line space, and the matrix \mathbf{K} is defined as:

$$\mathbf{K} = \begin{bmatrix} \frac{p_r}{f \cdot p_f} & 0 \\ 0 & \frac{l_r}{f \cdot l_f} \end{bmatrix}. \quad (10)$$

The unit-vector from the camera to the center of each pixel in the camera frame can be stated as:

$$\hat{\mathbf{a}}^C = \frac{1}{\sqrt{x^2 + y^2 + f^2}} \begin{bmatrix} x \\ y \\ f \end{bmatrix}. \quad (11)$$

^aDirection cosine matrices are defined as the rotation of bases:

$$\mathbf{R}_x = \begin{bmatrix} 1 & 0 & 0 \\ 0 & \cos\theta & \sin\theta \\ 0 & -\sin\theta & \cos\theta \end{bmatrix}, \quad \mathbf{R}_y = \begin{bmatrix} +\cos\theta & 0 & -\sin\theta \\ 0 & 1 & 0 \\ +\sin\theta & 0 & \cos\theta \end{bmatrix}, \quad \mathbf{R}_z = \begin{bmatrix} +\cos\theta & +\sin\theta & 0 \\ -\sin\theta & +\cos\theta & 0 \\ 0 & 0 & 1 \end{bmatrix}.$$

^bNote that each landmark measurement has the corresponding Earth-fixed landmark location vector, i.e., \mathbf{r}_{lmk}^B .

In this notation, mapped landmarks and the Earth-fixed camera position vector are related by:

$$\mathbf{r}^B + a \mathbf{R}_{IB} \hat{\mathbf{a}}^C = \mathbf{r}_{\text{lmk}}^B, \quad (12)$$

where $\mathbf{r}_{\text{lmk}}^B$ is the landmark location vector in the Earth-fixed frame. Note that $\hat{a}_3^C = f/\sqrt{x^2 + y^2 + f^2}$ and the following also holds true:

$$\begin{bmatrix} x \\ y \end{bmatrix} = \frac{f}{\hat{a}_3^C} \begin{bmatrix} \hat{a}_1^C \\ \hat{a}_2^C \end{bmatrix}. \quad (13)$$

With the above definitions, the partial derivative of pixel/line with respect to the Earth-fixed position vector can be stated as:

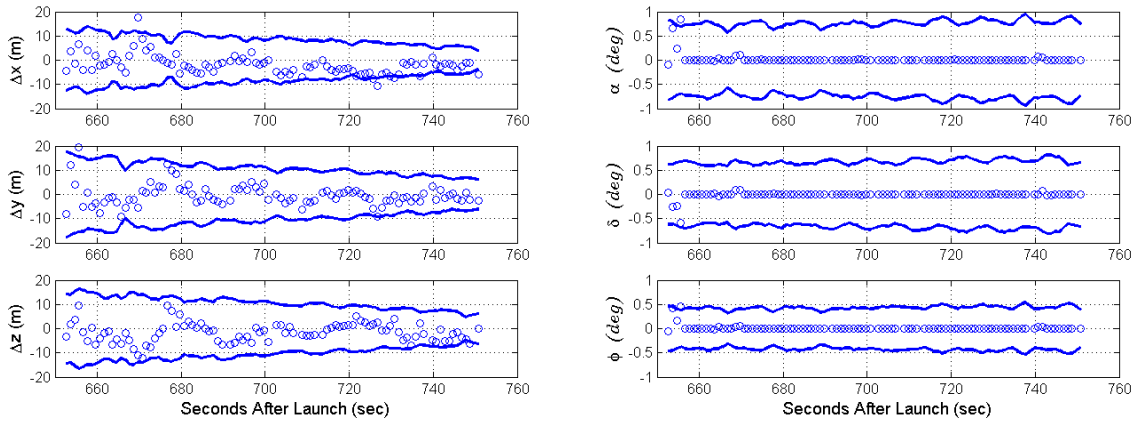
$$\frac{\partial(p_k, l_k)}{\partial \mathbf{r}^B} = -\mathbf{K} \left\{ \frac{f}{\hat{a}_3^C} \begin{bmatrix} \partial \hat{a}_1^C / \partial \mathbf{a}^C \\ \partial \hat{a}_2^C / \partial \mathbf{a}^C \end{bmatrix} - \frac{f}{(\hat{a}_3^C)^2} \begin{bmatrix} \hat{a}_1^C \\ \hat{a}_2^C \end{bmatrix} \frac{\partial \hat{a}_3^C}{\partial \mathbf{a}^C} \right\} \mathbf{R}_{CB}. \quad (14)$$

Moreover, the partial derivative of pixel/line with respect to the camera orientation angle can be stated as:

$$\frac{\partial(p, l)}{\partial(\alpha, \delta, \phi)} = \mathbf{K} \left\{ \frac{f}{\hat{a}_3^C} \begin{bmatrix} \partial \hat{a}_1^C / \partial \mathbf{a}^C \\ \partial \hat{a}_2^C / \partial \mathbf{a}^C \end{bmatrix} - \frac{f}{(\hat{a}_3^C)^2} \begin{bmatrix} \hat{a}_1^C \\ \hat{a}_2^C \end{bmatrix} \frac{\partial \hat{a}_3^C}{\partial \mathbf{a}^C} \right\} \frac{\partial [\mathbf{R}_z(\phi) \mathbf{R}_y(90^\circ - \delta) \mathbf{R}_z(\alpha) \mathbf{a}^1]}{\partial(\alpha, \delta, \phi)}. \quad (15)$$

Once these measurement partials are available, the Earth-fixed camera position vector and camera orientation angles can be solved iteratively.

Figures 4(a) and 4(b) show the kinematic-fix results compared with the GPS data. In this study, a total of 93 images (taken approximately every second) are processed and the number of landmarks per image ranged from 65 to 77. The position vector was initialized by using the first two landmark vectors, and the camera orientation was initialized from the dead-reckoned attitude using the IMU gyro data. Each pixel/line set is assigned 1 pixel accuracy and the *a priori* position and attitude uncertainties are assumed to be 10 km and 0.5 degrees.^c Figure 4(a) shows the position estimate with its 3- σ formal uncertainty. Overall, the position error agrees pretty well with the GPS data and the formal uncertainty is within the pin-point landing requirement. Figure 4(b) shows the kinematic-fix result of the attitude estimation. Since there is no truth attitude information from GPS, the camera orientation estimate is compared with the dead-reckoned attitude. The result shows sub-degree accuracy for the camera orientation.



(a) Difference between kinematic-fix and GPS positions in Cartesian (b) Difference between kinematic-fix and nominal camera orientations
EME2000 frame (circle) with 3- σ formal uncertainties (solid) (circle) with 3- σ formal uncertainties (solid).

Figure 4. Kinematic-fix of ST-9 landmark data.

^cAll *a priori* uncertainties assume 1- σ error.

IV. Full Trajectory Reconstruction

The full simulation is carried out using JPL’s legacy ODP software and is iterated until convergence is obtained. Note that the ODP is a pseudo-epoch state batch filter and that detailed algorithm descriptions can be found in the reference by Bierman.⁷ In the full simulation, the converted 50-Hz IMU accelerometer data is used in trajectory integration and the mapped landmark data is used to update the trajectory estimate. The estimation filter span started 649 seconds after launch and ended at 780 seconds after launch. Moreover, the same landmarks discussed in Section III.C are used, assuming $1\text{-}\sigma$ 1 pixel accuracy. The first image was taken at 653 seconds after launch (~ 1.5 km) and the last measurement was taken at 751 seconds after launch (~ 0.6 km).

The estimated parameters are the initial position and velocity, camera orientation of each image, and stochastic acceleration.^d The *a priori* position and velocity are initialized with a corresponding GPS state and the *a priori* camera orientations are initialized with the dead-reckoned attitude.^e Table IV shows the *a priori* uncertainties of the estimated parameters. In this study, the camera orientation angles are estimated as white stochastic parameters for each measurement point and the stochastic acceleration is estimated as a colored stochastic parameter with a 10 minute correlation time and a 20 second batch update time.

Table 1: *A priori* Uncertainties Used in Full Simulation ($1\text{-}\sigma$).

Initial Position (km)	Initial Velocity (m/s)	α, δ, ϕ (deg)	Stochastic Acceleration (m/s^2)
10	1	5	0.01

Figures 5(a) and 5(b) show the position and velocity errors when compared with the GPS data in the EME2000 frame. The result shows better than 10 meter position and 0.5 m/s velocity errors ($3\text{-}\sigma$) for the interval with available landmark data, which satisfies the pin-point landing requirement. Note that the discontinuities shown in Figure 5(a) are due to errors in the GPS data which can be improved by smoothing the GPS data, but this was not considered in this study. Figure 6(b) shows the estimated camera orientations with accuracy on the order of 0.1 degrees, which indicates fairly accurate nominal camera orientations. Figure 6(a) shows the stochastic acceleration estimates where ATAR is along the radial direction, ATAX is along the velocity direction, and ATAY completes the axes. The estimated stochastic acceleration uncertainty is much smaller when landmark measurements are available. Figures 7 and 8 show the position and velocity errors when images are taken at every 5 and 20 seconds. In all cases, the reconstructed position accuracies are better than 100 meters. This result indicates that the 100-meter pin-point landing requirement can be satisfied using IMU data and descent imagery with a batch filter.

V. Conclusion

The purpose of the 41.068 ST-9 sounding rocket experiment was to demonstrate the pin-point landing capability for future space missions. In this study, the raw ST-9 IMU accelerometer data were first converted into EME2000 inertial acceleration and were used in trajectory integration. The dead-reckoned trajectory using only the IMU data resulted in a large deviation (~ 2.3 km) at landing, which would not meet the pin-point landing requirement. To aid the trajectory accuracy, the descent images were pre-processed using the map-matching algorithm and landmarks were computed for each image. The kinematic-fix alone of the landmark measurements showed ~ 10 meter accuracy for the position estimates. This result indicated that trajectory reconstruction using both IMU data and descent images would satisfy the pin-point landing requirement.

In the full batch simulation, the estimated parameters were the spacecraft state, camera orientation angles, and stochastic accelerations. The reconstruction showed that the accuracy of the estimated position and velocity were on the order of few meters for the position and sub-meters per second for the velocity. Also, different landmark tracking update rates showed that imaging at a lower frequency (e.g., 20 seconds) can also satisfy the pin-point landing requirement. Overall, the reconstruction of the ST-9 sounding rocket trajectory showed that IMU data and descent imagery can be processed using a batch filter and can obtain the trajectory accuracy required for a pin-point landing at distant bodies.

^dStochastic acceleration assumes a constant acceleration over a certain batch interval, which can be correlated in time domain.

^eNote that this approach does not estimate the spacecraft attitude. The IMU gyro data is dead-reckoned only to rotate the IMU accelerometer data and to initialize the camera orientations.

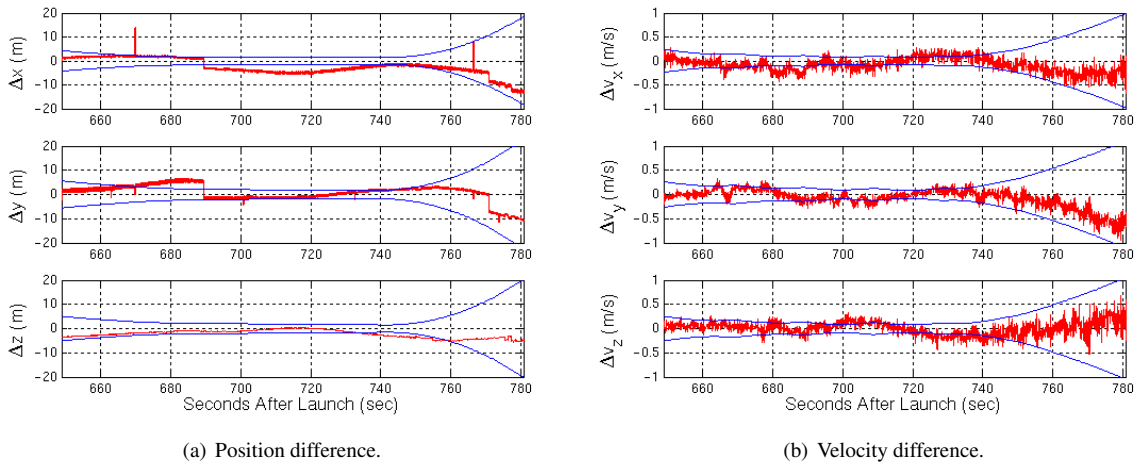


Figure 5. Difference between reconstructed trajectory and GPS data (red) with $3\text{-}\sigma$ formal uncertainty (blue). Images taken every 1 second.

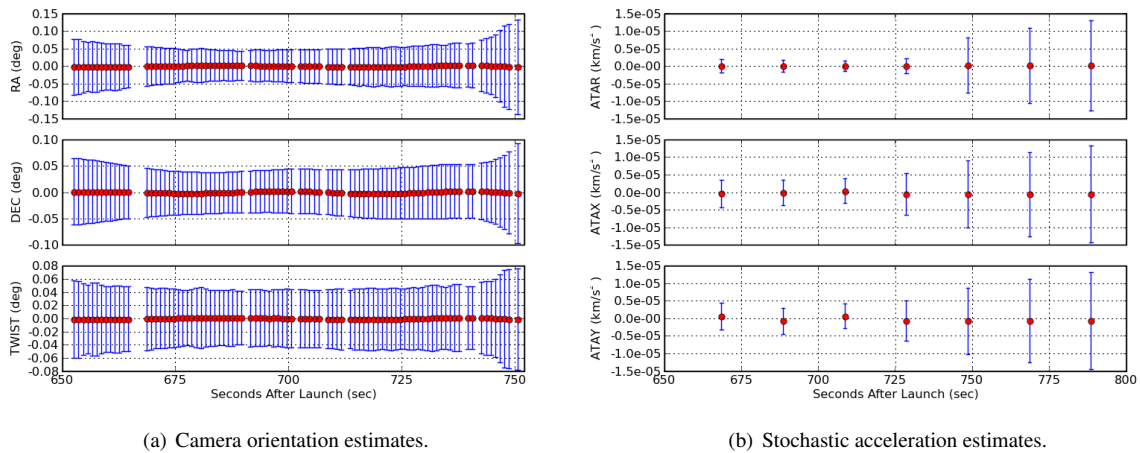


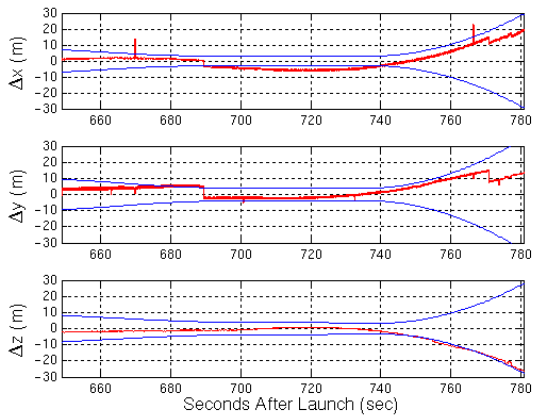
Figure 6. Difference between the estimated and nominal values (1 second).

VI. Acknowledgement

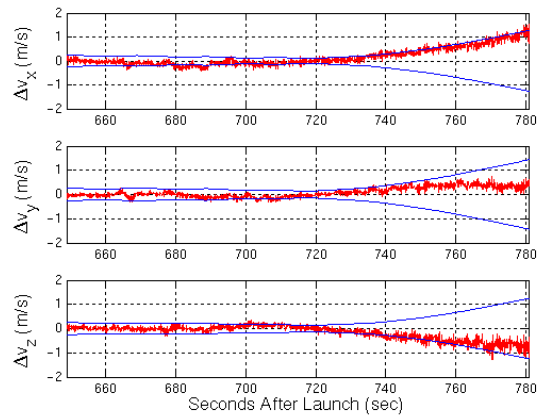
The research described in this paper was carried out at the Jet Propulsion Laboratory, California Institute of Technology, under a contract with the National Aeronautics and Space Administration. Copyright 2009 California Institute of Technology. Government sponsorship is acknowledged.

References

- ¹Wolf, A., Sklyanskiy, E., Tooley, J., and Rush, B., "Mars Pinpoint Landing System Trades," *Astrodynamics Specialist Conference*, August 2007, Mackinac Island, Michigan, AAS 07-310.
- ²Mourikis, A., Trawny, N., Roumeliotis, S., Johnson, A., Ansar, A., and Matthies, L., "Vision-Aided Inertial Navigation for Spacecraft Entry, Descent, and Landing," *IEEE Transactions on Robotics*, Vol. 25, No. 2, 2009, pp. 264–280.
- ³Wood, L., "The Evolution of Deep Space Navigation: 1962-1989," *31st Annual AAS Guidance and Control Conference*, February 2008, Breckenridge, Colorado, AAS 08-051.
- ⁴Desai, P., Prince, J., Queen, E., Cruz, J., and Grover, M., "Entry, Descent, and Landing Performance of the Mars Phoenix Lander," *Astrodynamics Specialist Conference*, August 2008, Honolulu, Hawaii, AIAA 2008-7346.
- ⁵Website: NGA EGM96 Geoid Calculator , <http://earth-info.nga.mil/GandG/wgs84/gravitymod/egm96/intpt.html>.
- ⁶Owen, W., *Optical Navigation Program Mathematical Models*, Jet Propulsion Laboratory Engineering Memorandum 343-2007-002, 2007.



(a) Position difference.

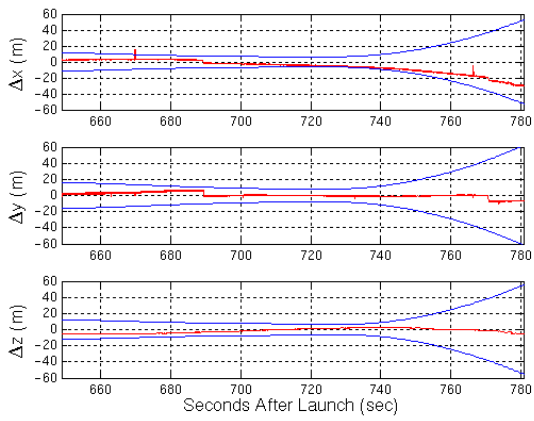


(b) Velocity difference.

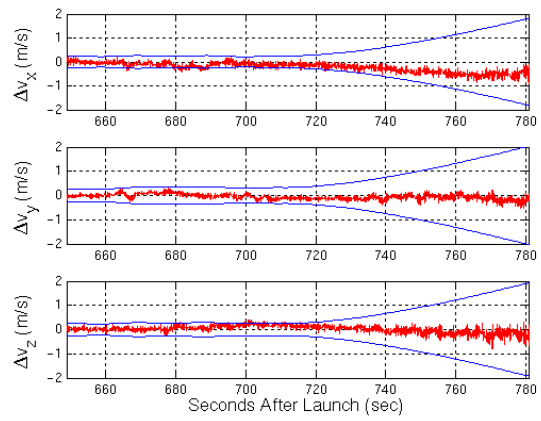
Figure 7. Difference between reconstructed trajectory and GPS data (red) with 3- σ formal uncertainty (blue). Images taken every 5 seconds.

⁷Bierman, G., *Factorization Methods for Discrete Sequential Estimation*, Vol. 128, Academic Press, 1977, pp. 13-32.

⁸Crassidis, J. and Junkins, J., *Optimal Estimation of Dynamics Systems*, CRC Press LLC, 2004, pp. 343-409.



(a) Position difference.



(b) Velocity difference.

Figure 8. Difference between reconstructed trajectory and GPS data (red) with $3\text{-}\sigma$ formal uncertainty (blue). Images taken every 20 seconds.